The molecular mechanism and evolutionary divergence of caspase 3/7-regulated gasdermin E activation

Hang Xu[1,2,3], Zihao Yuan[1,2], Kunpeng Qin[1,2,3], Shuai Jiang[1,2,3*], Li Sun[1,2,3*]

[1]*CAS and Shandong Province Key Laboratory of Experimental Marine Biology, Institute of Oceanology; CAS Center for Ocean Mega-Science, Chinese Academy of Sciences, Qingdao, China*

[2]*Laboratory for Marine Biology and Biotechnology, Pilot National Laboratory for Marine Science and Technology, Qingdao, China*

[3]*University of Chinese Academy of Sciences, Beijing, China*

*To whom correspondence should be addressed

Email: sjiang@qdio.ac.cn; lsun@qdio.ac.cn

Abstract

Cleavage of gasdermin, typically by caspase (CASP), is required for pyroptosis. In human, CASP3 and CASP7 recognize the same consensus motif DxxD, which is present in gasdermin E (GSDME), but only CASP3 cleaves GSDME. The underlying mechanism of this observation is unclear. In this study, we identified a pyroptotic pufferfish GSDME that was specifically cleaved by both pufferfish CASP3/7 and human CASP3/7. Domain swapping between pufferfish and human CASP/GSDME showed that the GSDME C-terminus and the CASP7 p10 subunit determined the cleavability of GSDME by CASP7. p10 contains a key residue that governs CASP7 substrate discrimination. This residue is highly conserved in vertebrate CASP3 and in most vertebrate (except mammalian) CASP7. In mammals, the key residue is conserved in non-primate (e.g., mouse) but not in primate. However, mouse CASP7 cleaved human GSDME but not mouse GSDME. These findings revealed the molecular mechanism of CASP7 substrate discrimination that underlies the evolutionary divergence of CASP3/7-mediated GSDME activation in vertebrate.

Key words

Immunity; Pyroptosis; Gasdermin E; Caspase 3; Caspase 7; Evolution

Introduction

Pyroptosis represents a necrotic form of programmed cell death that provokes robust inflammatory immune response (Bergsbaken, Fink, & Cookson, 2009; Tsuchiya et al., 2019). Gasdermin (GSDM) serves as the direct executioner of pyroptosis. GSDM forms transmembrane channels to permeabilize the cytoplasmic membrane, which leads to lytic cell death with massive release of proinflammatory cytokines (Kovacs & Miao, 2017; J. Shi, Gao, & Shao, 2017; Xia et al., 2021). Human has six GSDM family members, GSDMA-F (Tamura et al., 2007). All GSDMs (except for GSDMF) adopt a two-domain architecture, the N-terminal (NT) pore-forming domain and the C-terminal (CT) autoinhibitory domain (De Schutter et al., 2021; Shao, 2021). Proteolytic cleavage of GSDM to remove the autoinhibitory CT domain enables the binding of the lipophilic NT fragment to the cell membrane, where the NT fragments oligomerize and form transmembrane channels to induce osmotic cell lysis (Kuang et al., 2017; X. Liu et al., 2016).

Among the signaling pathways that activate GSDM-mediated pyroptosis, caspase (CASP) 1/4/5/11-mediated GSDMD activation is well documented. In human, GSDMD is specifically cleaved by the inflammatory CASP1 and the closely related CASP4/5 at the FLTD motif within the inter-domain linker region of GSDMD, and the cleavage unleashes the pore-forming GSDMD-NT fragment and triggers pyroptosis (He et al., 2015; Kayagaki et al., 2015; J. Shi et al., 2015). Structural and biochemical analysis reveal that CASP1/4 βIII/βIII' sheet forms an exosite that interacts with the hydrophobic pocket of GSDMD-CT domain, rendering GSDMD cleavage independent of CASP recognition of the tetrapeptide motif FLTD (K. Wang et al., 2020). When the tetrapeptide FLTD is mutated to AAAD, CASP1/4 cleavage of GSDMD is not affected. The residues that form the hydrophobic pocket of GSDMD-CT domain are not conserved in GSDME, suggesting that GSDME cannot be cleaved by CASP1/4 via interaction with an exosite (Z. Liu et al., 2020). Actually, human GSDME is specifically cleaved by CASP3 at the consensus motif DMPD, which is required for CASP3-

mediated GSDME proteolysis. Mutation of either the Asp residue of the DMPD tetrapeptide motif leads to cleavage resistance of GSDME (Rogers et al., 2017; Wang et al., 2017), indicating that CASP3-mediated GSDME activation paradigm is distinct from that of GSDMD. It is intriguing that although CASP7 shares the same recognition motif (DxxD) with CASP3, CASP7 cannot cleave GSDME (Agniswamy, Fang, & Weber, 2009; Slee, Adrain, & Martin, 2001). The molecular mechanism underlying the CASP3/7 cleavage discrimination of GSDME is unknown.

Historically, CASP3 and CASP7, which are 54% identical, are known to possess similar structure and share overlapping protein substrate repertoire, and are considered to have functionally redundant roles in regulating cell death (Crawford & Wells, 2011; Kumar, 2007; Y. Shi, 2002). Both CASP3 and CASP7 consist of two polypeptide subunits named p20 and p10 (1:1 ratio), which assemble to form active heterotetramer (Timmer & Salvesen, 2007). CASP3/7 contain highly conserved QACRG and SHG motifs in p20 subunit, and SWR and GSWF motifs in p10 subunit, which participate in the catalytic reaction and substrate binding, respectively (Boyce, Degterev, & Yuan, 2004; Cohen, 1997). In the apoptosis signaling pathway, death receptor-mediated extrinsic pathway and mitochondria-mediated intrinsic pathway ultimately converge to the activation of CASP3/7 (Budd, Tenneti, Lishnak, & Lipton, 2000; Wajant, 2002). Active CASP3/7 cleave a series of protein substrates, including poly(ADP-ribose) polymerase and DNA fragmentation factor 45, which causes chromatin fragmentation and leads to apoptosis (Erener et al., 2012; Wolf, Schuler, Echeverri, & Green, 1999; Zheng et al., 1998). Although CASP3 and CASP7 exert almost indistinguishable proteolytic specificity to certain polypeptides, there exist functional differences between these two CASPs in cleaving some substrates (Brentnall, Rodriguez-Menocal, De Guevara, Cepero, & Boise, 2013; Demon et al., 2009). For instance, CASP3 cleaves Bid much more efficiently than CASP7, while CASP7 cleaves cochaperone p23 more efficiently than CASP3 (Slee et al., 2001; Walsh et al., 2008). These findings support

the notion that CASP3 and CASP7 are enzymatically similar but functionally non-redundant.

Different from human GSDME that is specifically cleaved by CASP3, teleost GSDME is cleaved via various modes (Angosto-Bazarra et al., 2022; Yuan, Jiang, Qin, & Sun, 2022). In this study, we identified a functional GSDME (named TrGSDME) from pufferfish *Takifugu rubripes*. We found that TrGSDME was specifically cleaved by both human and pufferfish CASP3/7, whereas human GSDME was cleaved by pufferfish CASP3/7 and human CASP3, but not by human CASP7. We examined the underlying mechanism of this observation. We found that the GSDME-CT and the CASP7 p10 were critical for CASP7 cleavage of GSDME. By a series of site-directed mutagenesis, we discovered a previously unrecognized molecular determinant in p10 that was responsible for the discriminative cleavage of GSDME by CASP3/7.

Results

Pufferfish GSDME is specifically cleaved by both human and fish CASP3/7

It has long been observed that although human caspase (HsCASP) 3 and 7 share the same consensus recognition motif DxxD, HsCASP3, but not HsCASP7, cleaves human GSDME (HsGSDME) (at the site of DMPD). The underlying molecular mechanism is unknown. In this study, we found that pufferfish *Takifugu rubripes* GSDME (designated TrGSDME) was specifically cleaved by both HsCASP3 and 7 (Fig. 1A and B). This intriguing observation promoted us to explore the mechanism of CASP7 substrate discrimination. We first examined whether TrGSDME could be cleaved by pufferfish CASP (TrCASP) 3/7. The active forms of TrCASP3/7 were prepared (Fig. 1C), both exhibited high proteolytic specificity and activity towards the tetrapeptide DEVD (Fig. 1D and E), which is the conserved recognition motif of human CASP3/7. When incubated with TrGSDME, both TrCASP3 and TrCASP7 cleaved TrGSDME into the NT and CT fragments, similar to that cleaved by HsCASP3/7, in a dose

dependent manner (Fig. 1F and G). Accordingly, TrCASP3/7-mediated TrGSDME cleavage was inhibited by the CASP3 inhibitor (Z-DEVD-FMK) and the pan-CASP inhibitor (Z-VAD-FMK) (Fig. 1H). Based on the molecular mass of the cleaved NT and CT products, we inferred that the tetrapeptide motif ^{255}DAVD^{258} in the vicinity of the linker region of TrGSDME may be the recognition site of CASP3/7. Indeed, the D255R and D258A mutants of TrGSDME were resistant to TrCASP3/7 cleavage (Fig. 1I and J). Taken together, these results demonstrated that TrGSDME was cleaved by fish and human CASP3/7 in a manner that depended on the specific sequence of DAVD (Fig. 1K).

CASP3/7-cleaved TrGSDME is functionally activated and induces pyroptosis.

We next examined whether TrGSDME, like HsGSDME, is a functional pyroptosis inducer. For this purpose, HEK293T cells were transfected with mCherry-tagged full length (FL) or NT/CT domain of TrGSDME. Microscopy revealed that TrGSDME-FL and -CT were abundantly expressed in the cells, whereas TrGSDME-NT expression was barely detectable (Fig. 2A). No significant morphological change or LDH release was observed in cells expressing TrGSDME-FL or -CT (Fig. 2B and C). By contrast, cells expressing TrGSDME-NT showed necrotic cell death with massive LDH release (Fig. 2B and C). TrGSDME-NT-induced cell death exhibited osmotic cell membrane swelling, a typical feature of pyroptosis (Fig. 2D). Time-lapse imaging showed that TrGSDME-NT triggered rapid cell swelling and membrane rupture, which led to release of cytoplasmic contents and eventually cell death (Fig. 2E, Movie S1). To examine the pyroptotic activity of CASP3/7-cleaved TrGSDME, TrCASP3/7 and TrGSDME were overexpressed in HEK293T cells (Fig. 2F and G). The cells expressing TrCASP3, TrCASP7 or TrGSDME alone had no apparent morphological change or LDH release, whereas the cells co-expressing TrGSDME and TrCASP3 or TrGSDME and TrCASP7 underwent pyroptosis, accompanying with massive LDH release and TrGSDME cleavage (Fig. 2G-I). Consistently, the presence of the CASP3 inhibitor and pan-CASP inhibitor hampered TrGSDME-mediated pyroptosis (Fig. 2J and K).

Mutation of the cleavage site (D255R and D258A) inhibited pyroptosis and significantly decreased LDH release (Fig. 2L and M). These results indicated that CASP3/7 cleavage was required to activate TrGSDME-mediated pyroptosis.

GSDME-CT domain mediates the recognition by CASP7.

Since it is known that human GSDME is cleaved by CASP3 but not by CASP7, the observation that TrGSDME was cleaved by both human and fish CASP3/7 intrigued us to explore the underlying mechanism. We found that both HsCASP3 and 7 exhibited proteolytic activity towards the consensus CASP3/7 recognition motif, DMPD, in HsGSDME, but HsCASP7 failed to cleave HsGSDME (Fig. 3A and B). Sequence alignment revealed that compared to TrGSDME, HsGSDME possesses two additional regions with the possibility to form a β-strand (261-266 aa) and an α-helix (281-296 aa), respectively (Fig. 3C). We tested whether deletion of these two regions could confer HsCASP7 cleavage on HsGSDME. The results showed that similar to the wild type HsGSDME, the β-strand deletion mutant (Δ261-266) and the α-helix deletion mutant (Δ281-296) were cleaved by HsCASP3 but not by HsCASP7 (Fig. 3D). Since the NT and CT domains play different roles in GSDM structure maintenance, we constructed GSDME chimeras consisting of HsGSDME-NT plus TrGSDME-CT (named HsNT-TrCT), or TrGSDME-NT plus HsGSDME-CT (named TrNT-HsCT) (Fig. 3E). Compared with wild type HsGSDME and TrGSDME, chimeric HsNT-TrCT was cleaved by HsCASP3/7, whereas TrNT-HsCT was cleaved only by HsCASP3 (Fig. 3F-I), suggesting that the CT domain determined the cleavability of GSDME by HsCASP7.

The p10 subunit determines the substrate specificity of CASP7.

Since as shown above, unlike HsCASP7, TrCASP7 was able to cleave HsGSDME (Fig. 3H), we compared the sequences of TrCASP7 and HsCASP7. The two CASPs share 66.24% sequence identity. In these CASPs, the catalytic motifs SHG and QACRG in the p20 subunit and the substrate binding motifs SWR and GSWF in the p10 subunit

are conserved (Fig. 4A). To explore their substrate discrimination mechanism, we constructed CASP7 chimeras consisting of HsCASP7 p20 plus TrCASP7 p10 (named Hsp20-Trp10) or TrCASP7 p20 plus HsCASP7 p10 (named Trp20-Hsp10) (Fig. 4B, Fig. S1A). Compared to the wild types (HsCASP7 and TrCASP7), the chimeras exhibited comparable enzymatic activities towards the tetrapeptide substrates DAVD and DMPD (Fig. 4C). Like the wild types, both chimeras cleaved TrGSDME and HsNT-TrCT (Fig. 4D and E). By contrast, the Hsp20-Trp10 chimera cleaved HsGSDME, whereas the Trp20-Hsp10 chimera did not cleave HsGSDME (Fig. 4F). Similar cleavage pattern was observed towards TrNT-HsCT (Fig. 4G). These observations indicated that the p10 subunit dictated the cleavage specificity of CASP7 toward GSDME.

The S234 of p10 is the key to HsCASP7 discrimination on HsGSDME.

Comparative analysis of the p10 sequences of TrCASP7 and HsCASP7 identified 13 non-conserved residues. To examine their potential involvement in GSDME cleavage, a series of site-directed mutagenesis was performed to swap the non-conserved residues between HsCASP7 p10 and TrCASP7 p10 (Fig. 5A, Fig. S1B and C). Of the 13 swaps created, S234N conferred on HsCASP7 the ability to cleave HsGSDME (Fig. 5B), whereas its corresponding swap in TrCASP7 (N245S) markedly reduced the ability of TrCASP7 to cleave HsGSDME (Fig. 5C). None of the 13 swaps affected the ability of HsCASP7 or TrCASP7 to cleave TrGSDME (Fig. 5D, E). HsCASP7-S234N cleaved HsGSDME in a dose-dependent manner (Fig. 5F), and the cleavage was not enhanced by the additional mutation of S247N&I248V (Fig. 5G). Previous studies showed that human CASP1/4 cleaved GSDMD through exosite interaction (Z. Liu et al., 2020). To test whether there exists similar interaction between HsCASP7 and HsGSDME, three residues close to the corresponding CASP1/4 exosite in HsCASP7 were mutated (Q276W&D278E&H283S). Like the wild type, this mutant was unable to cleave HsGSDME (Fig. 5G), suggesting that, unlike human GSDMD, HsGSDME cleavage by CASPs probably did not involve exosite interaction. In contrast to HsGSDME,

TrGSDME cleavage by HsCASP7 was not affected by the mutation of S234N, S234N plus S247N&I248V, or Q276W&D278E&H283S (Fig. 5H).

All the above observed GSDME cleavages by CASP7 were verified in a cellular system. When co-expressed in HEK293T cells, HsGSDME was cleaved by TrCASP7 but not by HsCASP7, while TrGSDME was cleaved by both TrCASP7 and HsCASP7 (Fig. 5I and J). Additionally, both HsGSDME and TrGSDME were capable of cleaving by HsCASP7-S234N as well as TrCASP7-N245S (Fig. 5K and L). An apparent dose effect was observed in the cleavage of HsGSDME by HsCASP7-S234N (Fig. 5M).

Divergent and GSDME-independent evolution of CASP7 leads to its loss of GSDME-activation function in mammal.

Given the importance of N234 in p10 for CASP7 cleavage of GSDME, we analyzed the sequence conservation of this locus in CASP3/7. For CASP3, a highly conserved Asn residue (corresponding to HsCASP7 S234) was found immediately after the SWR motif in vertebrates (Fig. 6A and B). In HsCASP3, this conserved Asn is at position 208. We examined whether this residue was functionally essential to HsCASP3. Compared to the wild type, the N208S mutant exhibited much weaker cleavage of HsGSDME (Fig. 6C, Fig. S1D). Similar weakened cleavage was also observed in HEK293T cells co-expressing HsCASP3-N208S and HsGSDME (Fig. 6D). These results indicated that the Asn residue was also critical for HsCASP3 cleavage of HsGSDME.

For CASP7, an Asn at the position corresponding to HsCASP7 S234 is highly conserved in teleost, amphibians, reptiles and birds, but not in mammals (Fig. 6A). In mammals, the corresponding Asn is present in most non-primate species, such as mouse *Mus musculus* and bovine *Bos taurus*, but is replaced by Ser in primate, such as human *H. sapiens*, gorillas *Gorilla gorilla*, and chimpanzee *Pan troglodytes* (Fig. 6E, Fig. S2). We examined whether mouse CASP7 (MmCASP7) could cleave GSDME. The results showed that MmCASP7 cleaved HsGSDME in a dose-dependent manner, and the cleaving ability was abrogated by N234S mutation (Fig. 6G and H, Fig. S1E). By

contrast, neither MmCASP7 nor MmCASP7-N234S was able to cleave mouse GSDME (MmGSDME) (Fig. 6I). These results indicated the existence of an intra-species barrier for GSDME cleavage by CASP7 in some mammals, suggesting independent evolutions of CASP7 and GSDME.

Discussion

GSDME is an ancient member of the GSDM family existing ubiquitously in vertebrate from teleost to mammals (Broz, Pelegrin, & Shao, 2020; De Schutter et al., 2021). In human, GSDME is specifically cleaved by CASP3 at the consensus motif DMPD, but it is not cleaved by CASP7, which recognizes the same DxxD motif. CASP3 cleavage releases the pyroptosis-inducing NT fragment from the association of the inhibitory CT fragment and switches cell death from apoptosis to pyroptosis (Rogers et al., 2017; Wang et al., 2017). In this study, we found that different from human GSDME, pufferfish GSDME was specifically cleaved by both CASP3 and CASP7 at the site of DAVD to liberate the pyroptosis-inducing NT fragment. In teleost, there generally exist two GSDME orthologs, named GSDMEa and GSDMEb. In tongue sole *Cynoglossus semilaevis*, GSDMEb is preferably cleaved by CASP1 to trigger pyroptosis (Jiang, Gu, Zhao, & Sun, 2019). In zebrafish *Danio rerio*, GSDMEb is activated by caspy2 (CASP5 homolog) through the NLR family pyrin domain containing 3 (NLRP3) inflammasome signaling pathway (Li et al., 2020; Z. Wang et al., 2020). These observations indicate that similar to mammalian GSDMD, teleost GSDMEb is activated by inflammatory CASPs. In contrast, teleost GSDMEa is cleaved mainly by apoptotic CASPs. In zebrafish, GSDMEa is cleaved by CASP3 to generate the pyroptotic NT fragment (Wang et al., 2017). In turbot *Scophthalmus maximus*, GSDMEa is bi-directionally regulated by CASP3/7, which activate GSDMEa, and CASP6, which inactivates GSDMEa (Xu, Jiang, Yu, Yuan, & Sun, 2022). The complicated scenario of GSDME-mediated pyroptosis signaling in fish is likely due to the reason that, unlike mammals that have multiple GSDM members to induce pyroptosis under different conditions, fish have only GSDME to induce pyroptotic cell death. Regulation by different CASPs

may represent a mechanism that enables fish GSDME to execute the orders of different pyroptotic signals.

It is intriguing that, although HsCASP3 and 7 were indistinguishable in proteolysis towards the consensus tetrapeptide, they differed remarkably in the cleavage of HsGSDME and TrGSDME. HsCASP3, but not HsCASP7, cleaved HsGSDME, whereas both HsCASP3 and 7 cleaved TrGSDME at the same site. NT/CT domain swapping between HsGSDME and TrGSDME showed that chimeric GSDMEs containing the TrGSDME-CT domain were cleaved by human as well as pufferfish CASP7 regardless of the source of the NT, whereas chimeric GSDMEs containing the HsGSDME-CT domain were resistant to HsCASP7. These results indicate that the CT domain, which is well accepted to exert an inhibitory effect on the pore-forming NT domain (Z. Liu et al., 2019; J. Shi et al., 2015), is the target of HsCASP7 discrimination, and hence determines the cleavability of GSDME by HsCASP7. Recently, Wang and Liu studied the molecular mechanism of human GSDMD recognition by CASP1/4, and showed that GSDMD-CT interacted with CASP1/4 exosites through binding to a hydrophobic pocket, which enhanced the recognition by CASP1/4 and contributed to tetrapeptide sequence-independent cleavage of GSDMD (Z. Liu et al., 2020; K. Wang et al., 2020). Different from GSDMD, we found that for TrGSDME, mutation of either the P4 (D255) or P1 (D258) residue of the consensus motif ^{255}DAVD^{258} made it resistant to CASP3/7, implying a lack of DAVD-independent cleavage mechanism. Similarly, a previous study observed that human and mouse GSDME harboring cleavage site (P4 or P1) mutation resisted CASP3 cleavage (Wang et al., 2017). These results suggest that, compared to GSDMD, GSDME has a distinct enzyme-substrate engagement mode that, as demonstrated in the present study, involves GSDME-CT.

Unlike HsCASP7, which was unable to cleave HsGSDME, TrCASP7 effectively cleaved HsGSDME. The swapping of p20 between HsCASP7 and TrCASP7 revealed that the two catalytic motifs in p20, i.e., SHG and QACRG, were not involved in HsCASP7 discrimination on GSDME. SWR and GSWF are known to be responsible for CASP substrate binding (Chai et al., 2001; Riedl et al., 2001). However, in our

study, we found that these two motifs are conserved in human and pufferfish CASP7, and they had no apparent effect on the substrate discrimination of HsCASP7. By contrast, the chimeric HsCASP7 containing the p10 subunit of TrCASP7 acquired the ability to cleave HsGSDME, indicating an important role of p10. By a series of residue swapping and mutation analyses, we discovered that the residue in the position of 245 (in TrCASP7) or 234 (in HsCASP7) of the p10 subunit was the key that determined CASP7 cleavage of HsGSDME. Sequence analysis revealed that N245 is highly conserved in the CASP7 of teleost, amphibians, reptiles and birds, but not in the CASP7 of mammals, especially primates. With the exception of primates, the conserved Asn is present in a large number of mammals, including mice. Mouse CASP7 was able to cleave HsGSDME, further supporting the importance of the Asn in CASP7 recognition and cleavage. However, mouse CASP7 failed to cleave mouse GSDME, which is in accordance with the previous report that CASP7 deletion has little effect on mouse GSDME-mediated pyroptosis (Sarhan et al., 2018). These results suggest mutually independent evolution of GSDME and CASP7 in mice, which likely has distanced GSDME and CASP7 from each other. Similarly, human CASP7 and GSDME may also have undergone independent evolution, which leads to the disengagement of GSDME from the substrate relationship with CASP7.

In conclusion, we identified a teleost GSDME that can be cleaved by fish and human CASP3/7 to trigger pyroptosis. The GSDME-CT domain and the CASP7 p10 subunit are critical in the determination of CASP7 cleavage of GSDME. Within the p10 subunit, a single residue plays a key role in CASP7 substrate recognition and cleavage. Our results reveal the molecular basis of the functional divergence of CASP7 and CASP3, and suggest separate evolutions of CASP7 and GSDME in mammals. These findings add new insights into CASP-regulated GSDME activation in lower and higher vertebrates.

Materials and Methods

Animal, ethics, and cell line

Clinically healthy pufferfish (*Takifugu rubripes*) were obtained from a local fish farm. In the laboratory, the fish were maintained at 19-20℃ in aerated seawater as reported previously (Xu et al., 2022). For euthanization, the fish were immersed in excess tricaine methane sulfonate (Sigma, St. Louis, MO). The animal experiments were approved by the Ethics Committee of institute of Oceanology, Chinese Academy of Sciences. HEK293T cells (ATCC, Rockville, MD, USA) were cultured in DMED medium (Corning, NY, USA) supplemented with 10% fetal bovine serum (ExCell Bio, Shanghai, China) at 37℃ in a 5% CO_2 incubator.

Sequence analysis

The sequences of 742 CASP3 and 758 CASP7 used in this study were downloaded from NCBI Orthologs. TrCASP7 and HsCASP7 sequences were aligned with Clustal W program (www.ebi.ac.uk/clustalw/) and visualized with ESPript 3.0 (http://espript.ibcp.fr/ESPript/cgi-bin/ESPript.cgi/) (Robert & Gouet, 2014). Conservation of S/N234 in CASP3/7 was analyzed via Weblogo3 (https://weblogo.threeplusone.com/) (Crooks, Hon, Chandonia, & Brenner, 2004). The phylogenetic relationship of major mammalian clades was estimated based on the Mammals birth-death node-dated completed trees in VertLife (Upham, Esselstyn, & Jetz, 2019). The phylogenetic tree was subsequently viewed and edited in iTOL (Letunic & Bork, 2021). The icons representing phylogeny clades were retrieved from the PhyloPic (http://www.phylopic.org/), with the detailed credentials provided in Table S1.

Antibodies and immunoblotting

Monoclonal anti-mouse (ab215191) and anti-human (ab221843) GSDME antibodies were purchased from Abcam (Cambridge, MA). Antibodies against β-actin (AC026),

Flag (AE005), Myc (AE010), His (AE003), and mCherry (AE002) were purchased from Abclonal (Wuhang, China). Mouse polyclonal antibody against TrGSDME was prepared as reported previously (Xu et al., 2022). Immunoblotting was performed as reported previously (Zhao & Sun, 2022). Briefly, the samples were fractionated in 12% SDS-polyacrylamide gels (GenScript, Piscataway, NJ, USA). The proteins were transferred to NC membranes, immunobloted with appropriate antibodies and visualized using an ECL kit (Sparkjade Biotechnology Co. Ltd., Shandong, China).

Gene cloning and mutagenesis

Total RNA was extracted from pufferfish tissues using the FastPure Cell/Tissue Total RNA Isolation Kit V2 (Vazyme Biotech Co. Ltd., Nanjing, China). cDNA synthesis was performed with Revert Aid First Strand cDNA Synthesis Kit (Thermo Fisher Scientific, Waltham, MA, United States). The coding sequences (CDSs) of pufferfish GSDME and CASP3/7 were amplified by PCR. The CDSs of mouse GSDME and CASP7 were synthesized by Sangon Biotech (Shanghai, China). Site-directed mutagenesis was performed using Hieff Mut Site-Directed Mutagenesis Kit (Yeasen, Shanghai, China). Truncates of TrGSDME were created as reported previously (Xu et al., 2022) and subcloned into pmCherry-N1 (Clontech, Mountain View, CA, USA). For the construction of GSDME and CASP7 chimera, the CDSs of GSDME NT/CT and CASP7 p10/p20 were obtained by PCR and ligated into pET30a (+) (Novagen, Madison, WI, USA). All sequences/constructs were verified by sequencing analysis. The primers used are listed in Table S2.

Plasmids and transient expression

For expression in mammalian cell expression, the CDSs of GSDME (pufferfish, human and mouse) were subcloned into pCS2-3×Flag (Wang et al., 2017) or pmCherry-N1 and CDSs encoding CASP (pufferfish, human and mouse) were subcloned into p-CMV-Myc (Clontech, Mountain View, CA, USA) or pCS2-Myc (Wang et al., 2017). All plasmids were prepared with endotoxin-free plasmid kit (Sparkjade Biotechnology

Co. Ltd., Shandong, China). For transient expression, HEK293T cells were cultured in 96- or 24-well plates (Corning, NY, USA) overnight, then transfected with indicated plasmids with Liopfectamine 3000 (Invitrogen, USA). For GSDME processing, the plasmids of GSDME and CASP were co-transfected in HEK293T cells as described above and cultured continuously for 24 h. Cells were harvested and lysed with RIPA Lysis Buffer (Beyotime, Shanghai, China) for immunoblotting. The primer used are shown in Table S2.

Protein purification

Recombinant GSDMEs and CASPs were purified as described previously (Jiang, Zhou, Sun, Zhang, & Sun, 2020; Xu et al., 2022). Briefly, the CDSs of TrGSDME and CASP variants were each cloned into pET30a (+), and the CDSs of HsGSDME, MmGSDME, and chimeric GSDME were each cloned into pET28a-SUMO. The recombinant plasmids were introduced into *Escherichia coli* Transetta (DE3) (TransGen, Beijing, China) by transformation. The transformants were cultured in Luria broth (LB) at 37℃ until logarithmic growth phase. Isopropyl-β-D-thiogalactopyranoside (0.3 mM) was added to the medium, followed by incubation at 16℃ for 20 h. Bacteria were harvested and lysed, and the supernatant was collected for protein purification with Ni-NTA columns (GE Healthcare, Uppsala, Sweden). The proteins were dialyzed with PBS at 4 °C and concentrated.

CASP activity

To measure their proteolytic activity, recombinant CASPs were incubated separately with various colorimetric substrates as described previously (Jiang et al., 2020; Xu et al., 2022), and then monitored for released ρNA at OD405. To compare their substrate preference, TrCASP3/7 and HsCASP3/7 were incubated with Ac-DAVD-ρNA or Ac-DMPD-ρNA (Science Peptide Biological Technology Co., Ltd, shanghai, China) at 37℃ for 1 h, and the released ρNA was measured at OD405. The CASP activity in cells transfected TrCASP3/7 was determined as described previously (Xu et al., 2022).

GSDME cleavage by CASPs

GSDME cleavage assay was performed as described previously (Jiang et al., 2020; Xu et al., 2022). Briefly, recombinant GSDME was incubated with recombinant HsCASP1 ,2, 3, 6, 7, 8 and 9 (Enzo Life Sciences, Villeurbanne, France) at 37°C for 1 h in the reaction buffer (50 mM Hepes (pH 7.5), 3 mM EDTA, 150 mM NaCl, 0.005% (v/v) Tween 20, and 10 mM DTT). TrGSDME, HsGSDME or their chimeras were treated with TrCASP3/7, HsCASP3/7, or their chimeras for 2 h as above in reaction buffer. After incubation, the samples were boiled in 5 x Loading Buffer (GenScript, Piscataway, NJ, USA) and subjected to SDS-PAGE or immunoblotting with indicated antibody.

Cell death examination

Cell death examination by microscopy was performed as reported previously (Jiang et al., 2020; Xu et al., 2022). Briefly, HEK293T cells were plated into 35 mm glass-bottom culture dishes (Nest Biotechnology, Wuxi, China) at about 60% confluency and subjected to the indicated treatment. To examine cell death morphology, propidium iodide (PI) (Invitrogen, Carlsbad, CA, USA) and DiO (Solarbio, Beijing, China) were added to the culture medium, and the cells were observed with a Carl Zeiss LSM 710 confocal microscope (Carl Zeiss, Jena, Germany). To video the cell death process, the cells were transfected with pmCherry-N1 vector expressing TrGSDME-NT, and cell death was recorded using the above microscope. Cell death measured by lactate dehydrogenase (LDH) assay was performed as reported previously (Xu et al., 2022).

Statistical analysis

The Student's t test and one-way analysis of variance (ANOVA) were used for comparisons between groups. Statistical analysis was performed with GraphPad Prism 7 software. Statistical significance was defined as $P < 0.05$.

Acknowledgments

We thank Prof. Feng Shao (National institute of Biological Sciences, Beijing, China) for providing human CASP3/7 and GSDME expression vectors. This work was supported by the grants from the Science & Technology Innovation Project of Laoshan Laboratory (LSKJ202203000), the Youth Innovation Promotion Association CAS (2021204), the National Natural Science Foundation of China (41876175), and the Taishan Scholar Program of Shandong Province (2018 and 2021).

Author Contributions

Hang Xu: Methodology; Investigation; Visualization; Writing—original draft. ;**Zihao Yuan**: Investigation. **Kunpeng Qin**: Investigation; **Shuai Jiang**: Conceptualization; Methodology; Supervision; Writing—review & editing. **Li Sun**: Conceptualization; Supervision; Writing—review & editing.

Competing Interest Statement

The authors declare that they have no competing interests.

References

Agniswamy, J., Fang, B., & Weber, I. T. (2009). Conformational similarity in the activation of caspase-3 and -7 revealed by the unliganded and inhibited structures of caspase-7. *Apoptosis, 14*(10), 1135-1144. doi:10.1007/s10495-009-0388-9

Angosto-Bazarra, D., Alarcon-Vila, C., Hurtado-Navarro, L., Banos, M. C., Rivers-Auty, J., & Pelegrin, P. (2022). Evolutionary analyses of the gasdermin family suggest conserved roles in infection response despite loss of pore-forming functionality. *BMC Biol, 20*(1), 9. doi:10.1186/s12915-021-01220-z

Bergsbaken, T., Fink, S. L., & Cookson, B. T. (2009). Pyroptosis: host cell death and inflammation. *Nat Rev Microbiol, 7*(2), 99-109. doi:10.1038/nrmicro2070

Boyce, M., Degterev, A., & Yuan, J. (2004). Caspases: an ancient cellular sword of Damocles. *Cell Death Differ, 11*(1), 29-37. doi:10.1038/sj.cdd.4401339

Brentnall, M., Rodriguez-Menocal, L., De Guevara, R. L., Cepero, E., & Boise, L. H. (2013). Caspase-9, caspase-3 and caspase-7 have distinct roles during intrinsic apoptosis. *BMC Cell Biol, 14*, 32. doi:10.1186/1471-2121-14-32

Broz, P., Pelegrin, P., & Shao, F. (2020). The gasdermins, a protein family executing cell death and inflammation. *Nat Rev Immunol, 20*(3), 143-157. doi:10.1038/s41577-019-0228-2

Budd, S. L., Tenneti, L., Lishnak, T., & Lipton, S. A. (2000). Mitochondrial and extramitochondrial apoptotic signaling pathways in cerebrocortical neurons. *Proc Natl Acad Sci U S A, 97*(11), 6161-6166. doi:10.1073/pnas.100121097

Chai, J., Shiozaki, E., Srinivasula, S. M., Wu, Q., Datta, P., Alnemri, E. S., & Shi, Y. (2001). Structural basis of caspase-7 inhibition by XIAP. *Cell, 104*(5), 769-780. doi:10.1016/s0092-8674(01)00272-0

Cohen, G. M. (1997). Caspases: the executioners of apoptosis. *Biochem J, 326 (Pt 1)*, 1-16. doi:10.1042/bj3260001

Crawford, E. D., & Wells, J. A. (2011). Caspase substrates and cellular remodeling. *Annu Rev Biochem, 80*, 1055-1087. doi:10.1146/annurev-biochem-061809-121639

Crooks, G. E., Hon, G., Chandonia, J. M., & Brenner, S. E. (2004). WebLogo: a sequence logo generator. *Genome Res, 14*(6), 1188-1190. doi:10.1101/gr.849004

De Schutter, E., Roelandt, R., Riquet, F. B., Van Camp, G., Wullaert, A., & Vandenabeele, P. (2021). Punching Holes in Cellular Membranes: Biology and Evolution of Gasdermins. *Trends Cell Biol, 31*(6), 500-513. doi:10.1016/j.tcb.2021.03.004

Demon, D., Van Damme, P., Vanden Berghe, T., Deceuninck, A., Van Durme, J., Verspurten, J., . . . Vandenabeele, P. (2009). Proteome-wide substrate analysis

indicates substrate exclusion as a mechanism to generate caspase-7 versus caspase-3 specificity. *Mol Cell Proteomics, 8*(12), 2700-2714. doi:10.1074/mcp.M900310-MCP200

Erener, S., Petrilli, V., Kassner, I., Minotti, R., Castillo, R., Santoro, R., . . . Hottiger, M. O. (2012). Inflammasome-activated caspase 7 cleaves PARP1 to enhance the expression of a subset of NF-kappaB target genes. *Mol Cell, 46*(2), 200-211. doi:10.1016/j.molcel.2012.02.016

He, W. T., Wan, H., Hu, L., Chen, P., Wang, X., Huang, Z., . . . Han, J. (2015). Gasdermin D is an executor of pyroptosis and required for interleukin-1beta secretion. *Cell Res, 25*(12), 1285-1298. doi:10.1038/cr.2015.139

Jiang, S., Gu, H., Zhao, Y., & Sun, L. (2019). Teleost Gasdermin E Is Cleaved by Caspase 1, 3, and 7 and Induces Pyroptosis. *J Immunol, 203*(5), 1369-1382. doi:10.4049/jimmunol.1900383

Jiang, S., Zhou, Z., Sun, Y., Zhang, T., & Sun, L. (2020). Coral gasdermin triggers pyroptosis. *Sci Immunol, 5*(54). doi:10.1126/sciimmunol.abd2591

Kayagaki, N., Stowe, I. B., Lee, B. L., O'Rourke, K., Anderson, K., Warming, S., . . . Dixit, V. M. (2015). Caspase-11 cleaves gasdermin D for non-canonical inflammasome signalling. *Nature, 526*(7575), 666-671. doi:10.1038/nature15541

Kovacs, S. B., & Miao, E. A. (2017). Gasdermins: Effectors of Pyroptosis. *Trends Cell Biol, 27*(9), 673-684. doi:10.1016/j.tcb.2017.05.005

Kuang, S., Zheng, J., Yang, H., Li, S., Duan, S., Shen, Y., . . . Li, J. (2017). Structure insight of GSDMD reveals the basis of GSDMD autoinhibition in cell pyroptosis. *Proc Natl Acad Sci U S A, 114*(40), 10642-10647. doi:10.1073/pnas.1708194114

Kumar, S. (2007). Caspase function in programmed cell death. *Cell Death Differ, 14*(1), 32-43. doi:10.1038/sj.cdd.4402060

Letunic, I., & Bork, P. (2021). Interactive Tree Of Life (iTOL) v5: an online tool for phylogenetic tree display and annotation. *Nucleic Acids Res, 49*(W1), W293-W296. doi:10.1093/nar/gkab301

Li, J. Y., Wang, Y. Y., Shao, T., Fan, D. D., Lin, A. F., Xiang, L. X., & Shao, J. Z. (2020). The zebrafish NLRP3 inflammasome has functional roles in ASC-dependent interleukin-1beta maturation and gasdermin E-mediated pyroptosis. *J Biol Chem, 295*(4), 1120-1141. doi:10.1074/jbc.RA119.011751

Liu, X., Zhang, Z., Ruan, J., Pan, Y., Magupalli, V. G., Wu, H., & Lieberman, J. (2016). Inflammasome-activated gasdermin D causes pyroptosis by forming membrane pores. *Nature, 535*(7610), 153-158. doi:10.1038/nature18629

Liu, Z., Wang, C., Yang, J., Chen, Y., Zhou, B., Abbott, D. W., & Xiao, T. S. (2020). Caspase-1 Engages Full-Length Gasdermin D through Two Distinct Interfaces That Mediate Caspase Recruitment and Substrate Cleavage. *Immunity, 53*(1), 106-114 e105. doi:10.1016/j.immuni.2020.06.007

Liu, Z., Wang, C., Yang, J., Zhou, B., Yang, R., Ramachandran, R., . . . Xiao, T. S. (2019). Crystal Structures of the Full-Length Murine and Human Gasdermin D Reveal Mechanisms of Autoinhibition, Lipid Binding, and Oligomerization. *Immunity, 51*(1), 43-49 e44. doi:10.1016/j.immuni.2019.04.017

Riedl, S. J., Renatus, M., Schwarzenbacher, R., Zhou, Q., Sun, C., Fesik, S. W., . . . Salvesen, G. S. (2001). Structural basis for the inhibition of caspase-3 by XIAP. *Cell, 104*(5), 791-800. doi:10.1016/s0092-8674(01)00274-4

Robert, X., & Gouet, P. (2014). Deciphering key features in protein structures with the new ENDscript server. *Nucleic Acids Res, 42*(Web Server issue), W320-324. doi:10.1093/nar/gku316

Rogers, C., Fernandes-Alnemri, T., Mayes, L., Alnemri, D., Cingolani, G., & Alnemri, E. S. (2017). Cleavage of DFNA5 by caspase-3 during apoptosis mediates progression to secondary necrotic/pyroptotic cell death. *Nat Commun, 8*, 14128. doi:10.1038/ncomms14128

Sarhan, J., Liu, B. C., Muendlein, H. I., Li, P., Nilson, R., Tang, A. Y., . . . Poltorak, A. (2018). Caspase-8 induces cleavage of gasdermin D to elicit pyroptosis during Yersinia infection. *Proc Natl Acad Sci U S A, 115*(46), E10888-E10897. doi:10.1073/pnas.1809548115

Shao, F. (2021). Gasdermins: making pores for pyroptosis. *Nat Rev Immunol, 21*(10), 620-621. doi:10.1038/s41577-021-00602-2

Shi, J., Gao, W., & Shao, F. (2017). Pyroptosis: Gasdermin-Mediated Programmed Necrotic Cell Death. *Trends Biochem Sci, 42*(4), 245-254. doi:10.1016/j.tibs.2016.10.004

Shi, J., Zhao, Y., Wang, K., Shi, X., Wang, Y., Huang, H., . . . Shao, F. (2015). Cleavage of GSDMD by inflammatory caspases determines pyroptotic cell death. *Nature, 526*(7575), 660-665. doi:10.1038/nature15514

Shi, Y. (2002). Mechanisms of caspase activation and inhibition during apoptosis. *Mol Cell, 9*(3), 459-470. doi:10.1016/s1097-2765(02)00482-3

Slee, E. A., Adrain, C., & Martin, S. J. (2001). Executioner caspase-3, -6, and -7 perform distinct, non-redundant roles during the demolition phase of apoptosis. *J Biol Chem, 276*(10), 7320-7326. doi:10.1074/jbc.M008363200

Tamura, M., Tanaka, S., Fujii, T., Aoki, A., Komiyama, H., Ezawa, K., . . . Shiroishi, T. (2007). Members of a novel gene family, Gsdm, are expressed exclusively in the epithelium of the skin and gastrointestinal tract in a highly tissue-specific manner. *Genomics, 89*(5), 618-629. doi:10.1016/j.ygeno.2007.01.003

Timmer, J. C., & Salvesen, G. S. (2007). Caspase substrates. *Cell Death Differ, 14*(1), 66-72. doi:10.1038/sj.cdd.4402059

Tsuchiya, K., Nakajima, S., Hosojima, S., Thi Nguyen, D., Hattori, T., Manh Le, T., . . . Suda, T. (2019). Caspase-1 initiates apoptosis in the absence of gasdermin D. *Nat Commun, 10*(1), 2091. doi:10.1038/s41467-019-09753-2

Upham, N. S., Esselstyn, J. A., & Jetz, W. (2019). Inferring the mammal tree: Species-level sets of phylogenies for questions in ecology, evolution, and conservation. *PLoS Biol, 17*(12), e3000494. doi:10.1371/journal.pbio.3000494

Wajant, H. (2002). The Fas signaling pathway: more than a paradigm. *Science, 296*(5573), 1635-1636. doi:10.1126/science.1071553

Walsh, J. G., Cullen, S. P., Sheridan, C., Luthi, A. U., Gerner, C., & Martin, S. J. (2008). Executioner caspase-3 and caspase-7 are functionally distinct proteases. *Proc Natl Acad Sci U S A, 105*(35), 12815-12819. doi:10.1073/pnas.0707715105

Wang, K., Sun, Q., Zhong, X., Zeng, M., Zeng, H., Shi, X., . . . Ding, J. (2020). Structural Mechanism for GSDMD Targeting by Autoprocessed Caspases in Pyroptosis. *Cell, 180*(5), 941-955 e920. doi:10.1016/j.cell.2020.02.002

Wang, Y., Gao, W., Shi, X., Ding, J., Liu, W., He, H., . . . Shao, F. (2017). Chemotherapy drugs induce pyroptosis through caspase-3 cleavage of a gasdermin. *Nature, 547*(7661), 99-103. doi:10.1038/nature22393

Wang, Z., Gu, Z., Hou, Q., Chen, W., Mu, D., Zhang, Y., . . . Yang, D. (2020). Zebrafish GSDMEb Cleavage-Gated Pyroptosis Drives Septic Acute Kidney Injury In Vivo. *J Immunol, 204*(7), 1929-1942. doi:10.4049/jimmunol.1901456

Wolf, B. B., Schuler, M., Echeverri, F., & Green, D. R. (1999). Caspase-3 is the primary activator of apoptotic DNA fragmentation via DNA fragmentation factor-45/inhibitor of caspase-activated DNase inactivation. *J Biol Chem, 274*(43), 30651-30656. doi:10.1074/jbc.274.43.30651

Xia, S., Zhang, Z., Magupalli, V. G., Pablo, J. L., Dong, Y., Vora, S. M., . . . Wu, H. (2021). Gasdermin D pore structure reveals preferential release of mature interleukin-1. *Nature*. doi:10.1038/s41586-021-03478-3

Xu, H., Jiang, S., Yu, C., Yuan, Z., & Sun, L. (2022). GSDMEa-mediated pyroptosis is bi-directionally regulated by caspase and required for effective bacterial clearance in teleost. *Cell Death Dis, 13*(5), 491. doi:10.1038/s41419-022-04896-5

Yuan, Z., Jiang, S., Qin, K., & Sun, L. (2022). New insights into the evolutionary dynamic and lineage divergence of gasdermin E in metazoa. *Front Cell Dev Biol, 10*, 952015. doi:10.3389/fcell.2022.952015

Zhao, Y., & Sun, L. (2022). Bacillus cereus cytotoxin K triggers gasdermin D-dependent pyroptosis. *Cell Death Discov, 8*(1), 305. doi:10.1038/s41420-022-01091-5

Zheng, T. S., Schlosser, S. F., Dao, T., Hingorani, R., Crispe, I. N., Boyer, J. L., & Flavell, R. A. (1998). Caspase-3 controls both cytoplasmic and nuclear events associated with Fas-mediated apoptosis in vivo. *Proc Natl Acad Sci U S A, 95*(23), 13618-13623. doi:10.1073/pnas.95.23.13618

Figure legends

Figure 1. Cleavage of TrGSDME by caspases. (A, B) TrGSDME was treated with different HsCASPs and then subjected to SDS-PAGE (A) and immunoblotting (B). **(C)** SDS-PAGE analysis of purified TrCASP3/7. The p10 and p20 subunits are indicated. **(D)** TrCASP3/7 cleavage of different colorimetric CASP substrates was monitored by measuring released ρNA. The values are the means ± SD of three replicates. **(E)** TrCASP3/7 (0.25-8U) were incubated with Ac-DEVD-ρNA, and time-dependent release of ρNA was measured. **(F, G)** SDS-PAGE (F) and immunoblotting (G) analysis of TrGSDME cleavage by TrCASP3/7 (0.25-4U). **(H)** TrGSDME cleavage by TrCASP3/7 was determined in the presence or absence of Z-DEVD-FMK or Z-VAD-FMK. **(I, J)** TrGSDME wild type (WT) and mutants (D255R or D258A) were incubated with TrCASP3/7, and the cleavage was determined by SDS-PAGE (I) and immunoblotting (J). **(K)** A schematic of TrGSDME cleavage by TrCASP3/7. The arrow indicates cleavage site. For all panels, FL, full length; NT, N-terminal fragment; CT, C-terminal fragment.

Figure 2. The pyroptotic activity of TrGSDME. (A-C) HEK293T cells expressing mCherry-tagged TrGSDME full length (FL) or truncates (NT or CT) were analyzed for TrGSDME expression (A), morphological change (B) and LDH release (C). Scale bars, 50 μm (A) and 20 μm (B). **(D)** HKE293T cells were transfected with the backbone vector or vector expressing Myc-tagged TrGSDME-NT. The cell nuclei and membrane were stained with PI and DiO, respectively. Scale bar, 10 μm. **(E)** HEK293T cells were transfected with mCherry-tagged TrGSDME-NT, and the progression of cell death was shown by time-lapse microscopic imaging. Scale bar, 10 μm. **(F)** HEK293T cells were transfected with TrCASP3/7, and the proteolytic activity of TrCASP3/7 was assessed

by treatment with fluorogenic Ac-DEVD-AFC. **(G)** Phase-contrast images of HEK293T cells transfected with the indicated vectors. Scale bar, 20 μm. **(H, I)** LDH release (H) and TrGSDME cleavage (I) in the above transfected cells were determined. For panel (I), FL, full-length; CT, C-terminal fragment. **(J, K)** HKE293T cells co-expressing TrGSDME and TrCASP3/7 in the presence or absence (control) of Z-VAD-FMK or Z-DEVD-FMK were subjected to microscopy (J) and LDH measurement (K). Scale bar, 20 μm. **(L, M)** HEK293T cells expressing TrCASP3/7 plus TrGSDME or TrCASP3/7 plus the D255R/D258A mutant were subjected to microscopy (L) and LDH measurement (M). Scale bar, 20 μm. For panels (C, F, H, K and M), values are the means of three experimental replicates and shown as means ± SD. $^{**}P < 0.01$, $^{***}P < 0.001$.

Figure 3. GSDME-CT domain determines the recognition by CASP7. (A) HsGSDME was treated with various HsCASPs, and the products were analyzed by immunoblotting with anti-HsGSDME-CT antibody. **(B)** HsCASP3/7 and TrCASP3/7 were incubated with Ac-DAVD-ρNA or Ac-DMPD-ρNA, and the proteolytic activity was determined. Data are expressed as the means ± SD of three replicates. **(C)** Sequence alignment of the linker region from HsGSDME and TrGSDME. Two regions that may form α-helix and β-strand are indicated. **(D)** HsGSDME wild type (WT) and mutants (Δ261-266 and Δ281-296) were treated with or without HsCASP3/7, and the cleaved fragments were subjected to immunoblotting with anti-HsGSDME-CT antibody. **(E)** Schematics of the chimeric GSDME constructs. **(F-I)** TrGSDME (F), HsNT-TrCT (G), HsGSDME (H) and TrNT-HsCT (I) were incubated with TrCASP3/7 or HsCASP3/7, and the cleavage was determined by immunoblotting with anti-TrGSDME or anti-HsGSDME-CT antibodies. For panels (A, D, and F-I): FL, full length; NT, N-terminal fragment; CT, C-terminal fragment.

Figure 4. The p10 subunit of CASP7 is essential for discrimination on GSDME. (A) Sequence alignment of HsCASP7 and TrCASP7. α-helices and β-strands are indicated. The motifs involved in catalytic reaction (SHG and QACRG) and substrate binding (SWR and GSWF) are boxed in red. **(B)** Schematics of CASP7 chimeras. **(C)**

The proteolytic activities of TrCASP7, HsCASP7 and their chimeras were determined by cleaving Ac-DAVD-ρNA and Ac-DMPD-ρNA. Data are expressed as the means ± SD of three replicates. **(D-G)** TrGSDME (D), HsNT-TrCT (E), HsGSDME (F) or TrNT-HsCT (G) were incubated with TrCASP7, HsCASP7 and their chimeras. The products were assessed by immunoblotting with anti-TrGSDME or anti-HsGSDME-CT antibodies. For panels (D-G): FL, full length; NT, N-terminal fragment; CT, C-terminal fragment.

Figure 5. Functional importance of the non-conserved residues in the p10 of HsCASP7 and TrCASP7. (A) Sequence alignment of the p10 region in HsCASP7 and TrCASP7. The arrows indicate non-conserved residues. **(B, C)** HsGSDME was treated with wild type (WT) or mutant HsCASP7 (B) or TrCASP7 (C). The cleavage was determined by immunoblotting with anti-HsGSDME-CT antibody. 205TME, HsCASP7 with TME insertion at position 205; 213ΔTME, TrCASP7 with TME deleted at position 213. **(D, E)** TrGSDME was incubated with wild type (WT) or mutant HsCASP7 (D) or TrCASP7 (E). The cleavage was determined by immunoblotting with anti-TrGSDME antibody. **(F)** HsGSDME was incubated with HsCASP7 or the S234N mutant (0.25-4U). HsGSDME cleavage was analyzed as above. **(G, H)** HsGSDME (G) and TrGSDME (H) were treated with wild type or mutant HsCASP7. The cleavage was determined as above. **(I, J)** TrGSDME (I) or HsGSDME (J) was co-expressed with different doses of TrCASP7/HsCASP7 in HEK293T cells. GSDME cleavage, CASP7 and β-actin were determined by immunoblotting. **(K, L)** TrGSDME (K) or HsGSDME (L) was co-expressed with wild type or mutant TrCASP7/HsCASP7. GSDME cleavage, CASP7 and β-actin were determined as above. **(M)** HsGSDME was co-expressed with HsCASP7 or HsCASP7-S234N. Cleavage of GSDME was detected as above. For panels (B-M): FL, full length; NT, N-terminal fragment; CT, C-terminal fragment.

Figure 6. Conservation and functional importance of S/N234 in CASP3/7. (A) Weblogo analysis of the conservation of S/N234 in CASP3/7 in Mammalia, Aves, Reptilia, Amphibia and Osteichthyes. **(B)** Sequence alignment of HsCASP3/7. The S/N residues are indicated by red arrow. **(C)** HsGSDME was treated with HsCASP3 or

HsCASP3-N208S, and then subjected to immunoblotting with anti-HsGSDME-CT antibody. **(D)** HsGSDME was co-expressed in HEK293T cells with different doses of HsCASP3 or HsCASP3-N208S. The cell lysates were immunoblotted to detect HsGSDME, CASP3, and β-actin. **(E)** Sequence alignment of the S/N234 region in the CASP7 of primate (shaded cyan) and non-primate mammals. The S/N residues are indicated by red arrow. Asterisks indicate identical residues. **(F)** Alignment of human and mouse CASP7 sequences. The S/N234 residues are indicated by arrow. **(G)** HsGSDME was treated with different units of HsCASP7 or MmCASP7, and the cleavage was assessed by immunoblotting with anti-HsGSDME-CT antibody. **(H)** HsGSDME was incubated with different units of MmCASP7 or its mutant (N234S), and HsGSMDE cleavage was analyzed as above. **(I)** MmCASP7 was treated with HsCASP7, MmCASP7 or MmCASP7-N234S. The cleavage was determined by immunoblotting with anti-MmGSDME-NT antibody. For panels (C, D, and G-I), FL, full length; NT, N-terminal fragment; CT, C-terminal fragment.

Figures

Figure 1

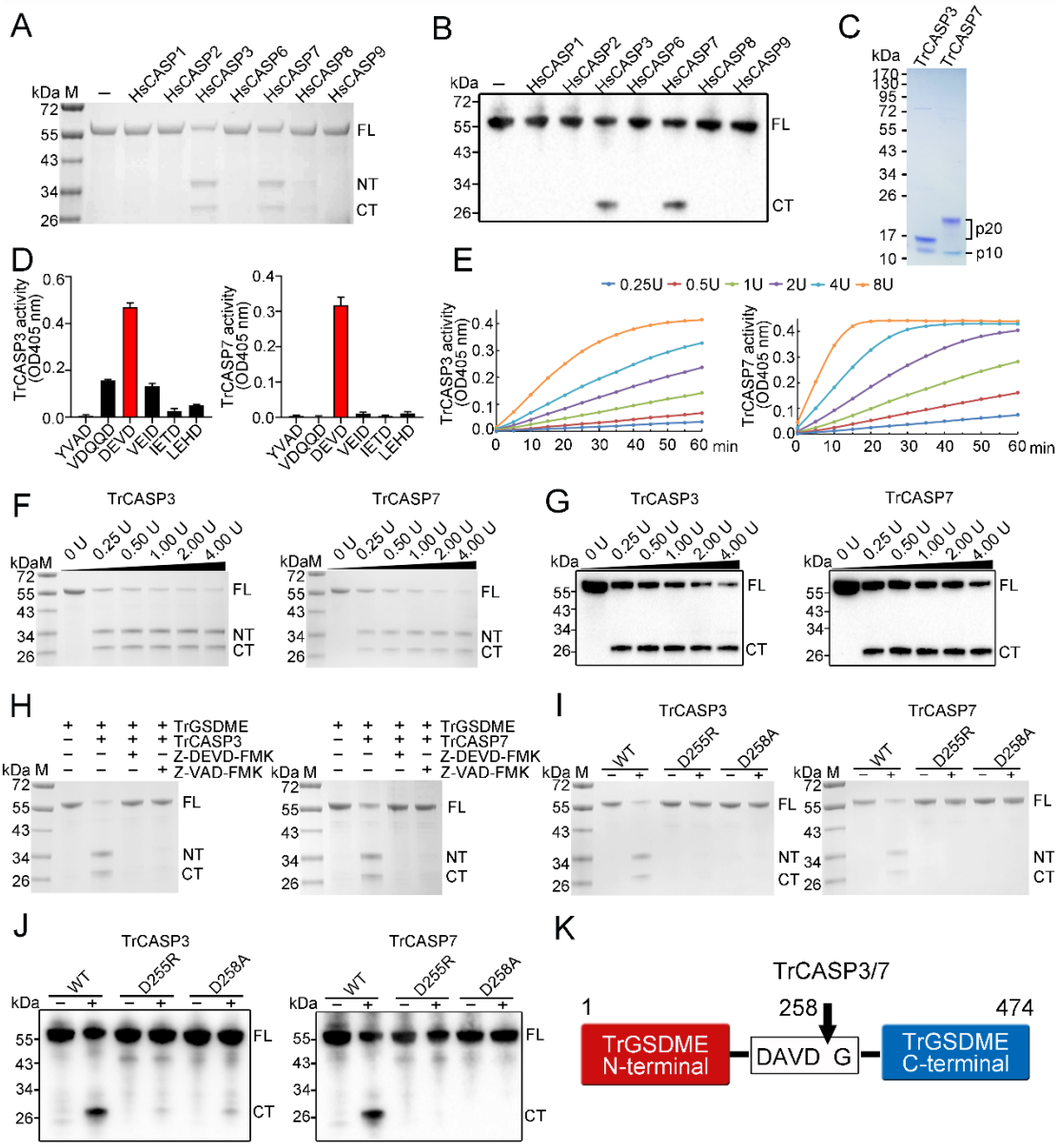

Figure 2

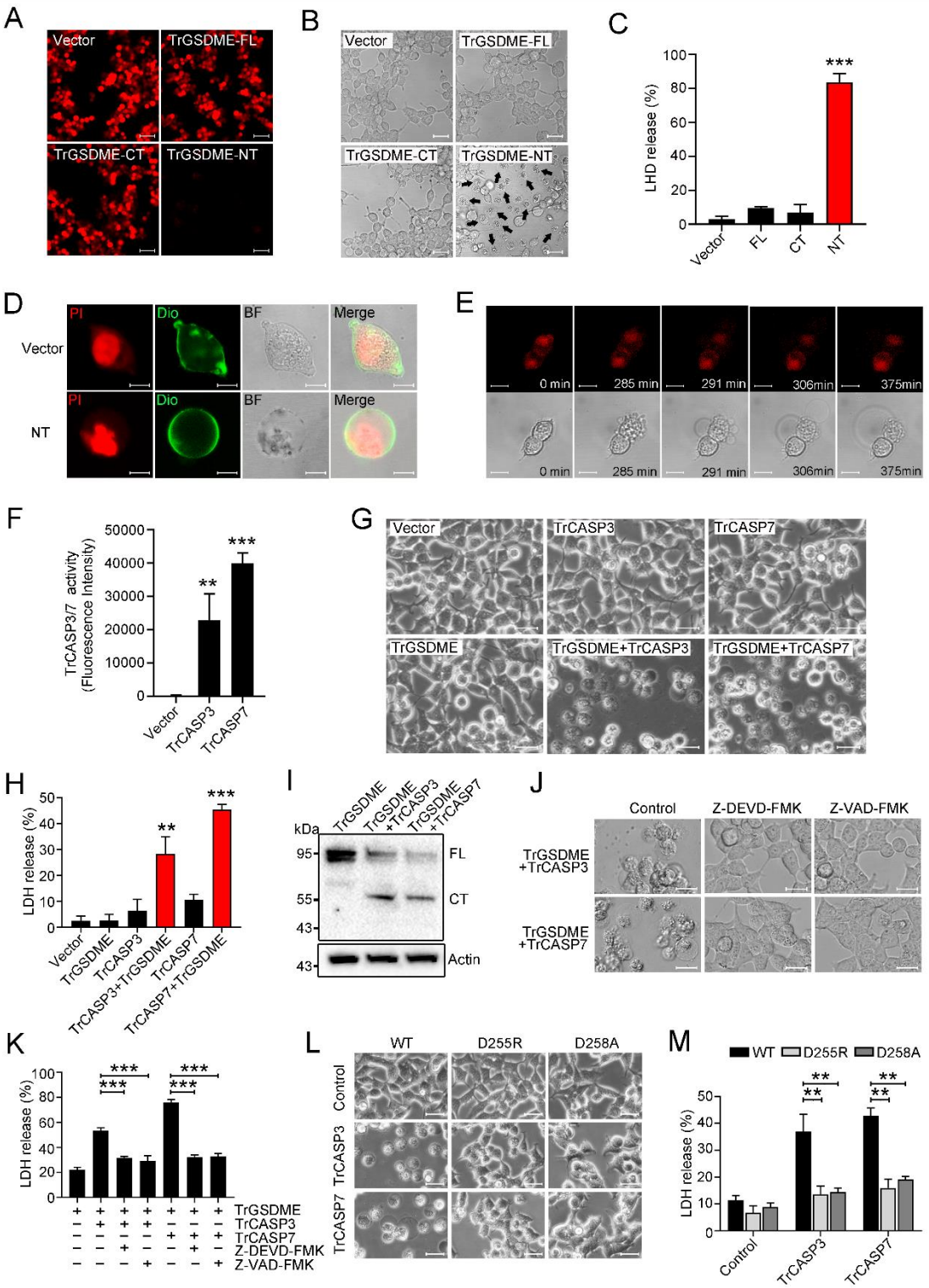

707

708

Figure 3

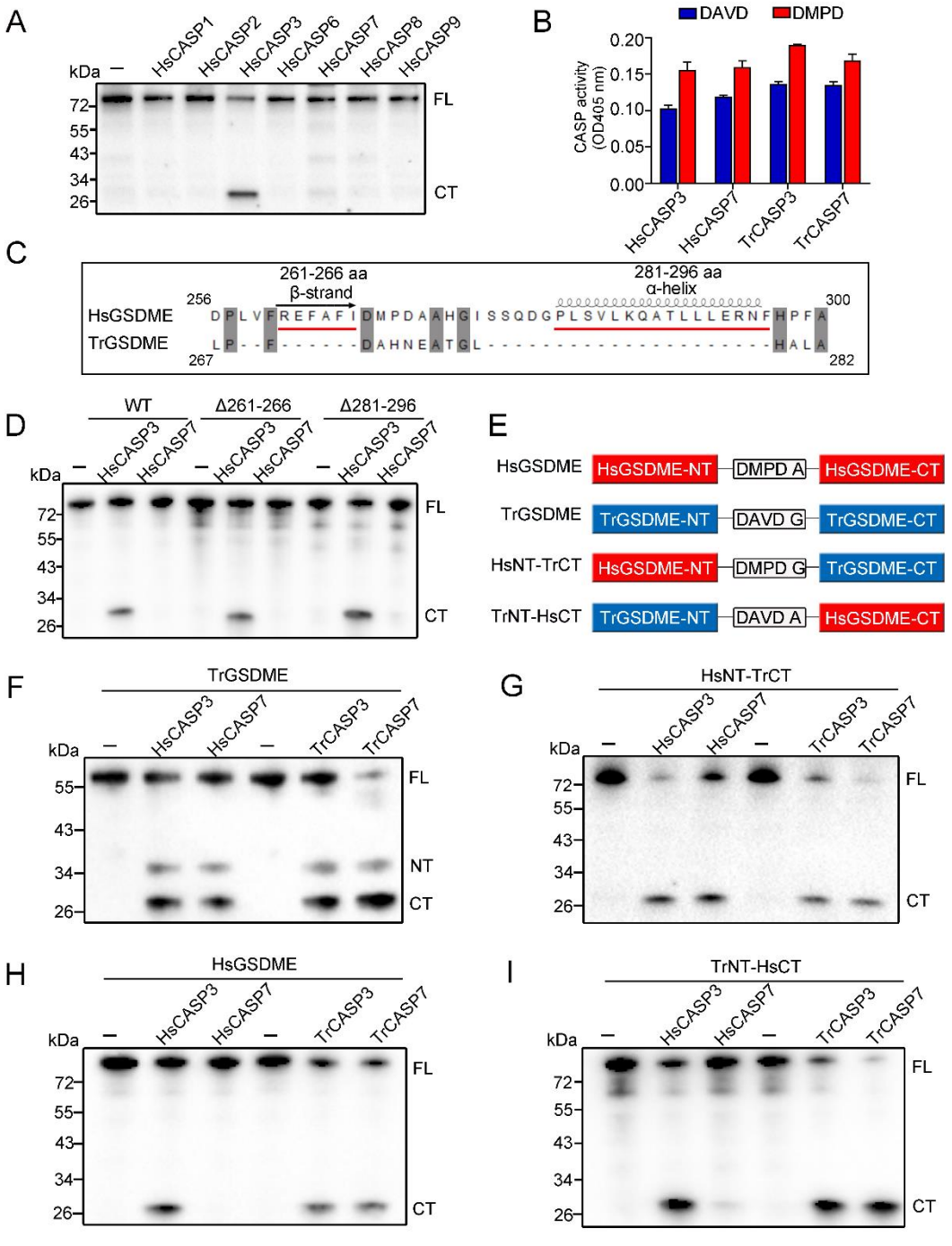
A
kDa
–
HsCASP1
HsCASP2
HsCASP3
HsCASP6
HsCASP7
HsCASP8
HsCASP9
72
55
43
34
26
FL
CT
B
DAVD
DMPD
CASP activity (OD405 nm)
0.20
0.15
0.10
0.05
0.00
HsCASP3
HsCASP7
TrCASP3
TrCASP7
C
261-266 aa
β-strand
281-296 aa
α-helix
256
300
HsGSDME
TrGSDME
267
282
D
WT
Δ261-266
Δ281-296
HsCASP3
HsCASP7
E
HsGSDME
HsGSDME-NT
DMPD A
HsGSDME-CT
TrGSDME
TrGSDME-NT
DAVD G
TrGSDME-CT
HsNT-TrCT
DMPD G
TrNT-HsCT
DAVD A
F
TrGSDME
TrCASP3
TrCASP7
NT
G
HsNT-TrCT
H
HsGSDME
I
TrNT-HsCT

Figure 4

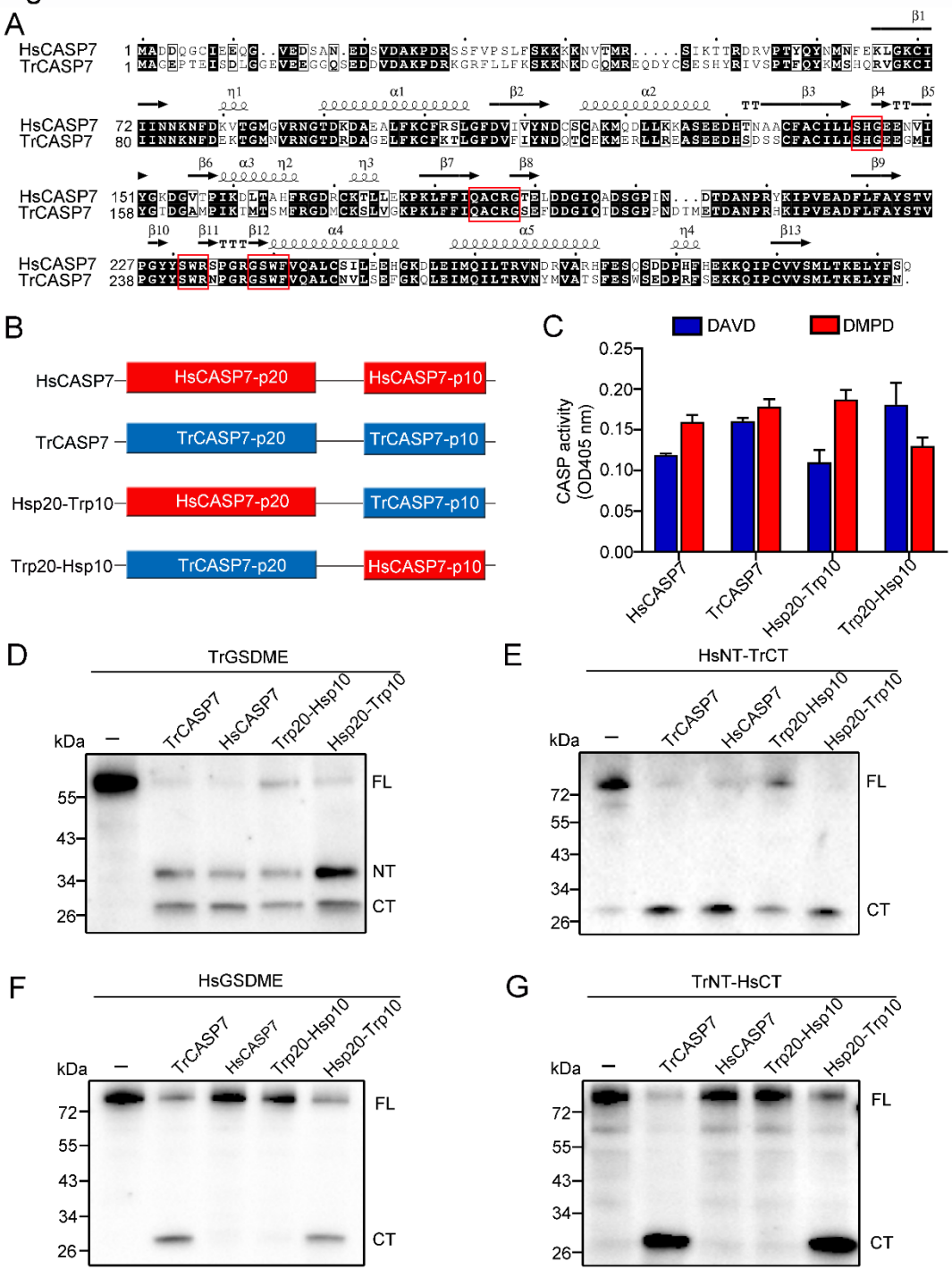
A
HsCASP7
TrCASP7
B
HsCASP7
HsCASP7-p20
HsCASP7-p10
TrCASP7
TrCASP7-p20
TrCASP7-p10
Hsp20-Trp10
Trp20-Hsp10
C
DAVD
DMPD
CASP activity (OD405 nm)
0.25
0.20
0.15
0.10
0.05
0.00
HsCASP7
TrCASP7
Hsp20-Trp10
Trp20-Hsp10
D
TrGSDME
E
HsNT-TrCT
F
HsGSDME
G
TrNT-HsCT
kDa
–
TrCASP7
HsCASP7
Trp20-Hsp10
Hsp20-Trp10
FL
NT
CT
55
43
34
26
72

Figure 5

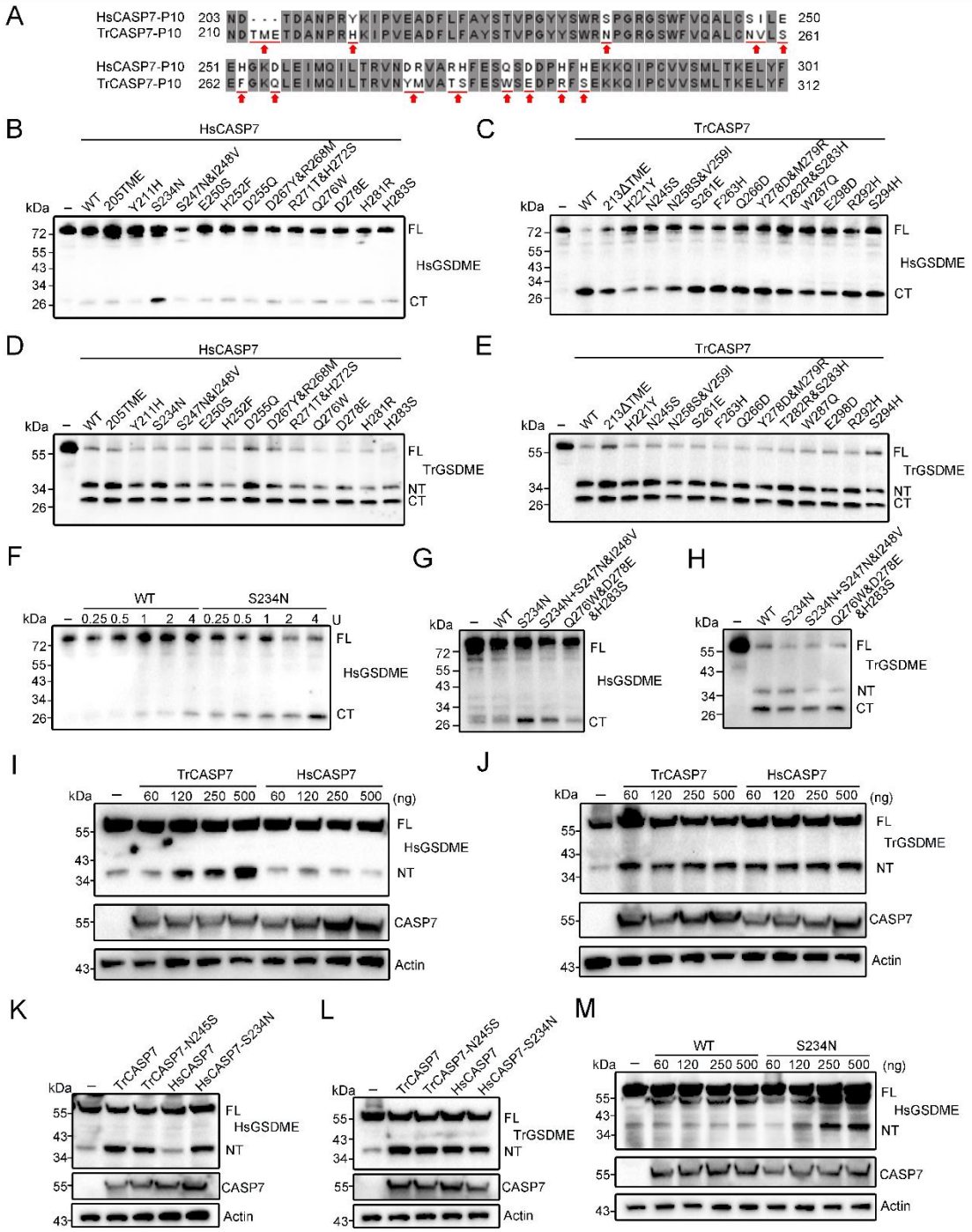
A
HsCASP7-P10 203 ND - - - TDANPRYKIPVEADFLFAYSTVPGYYSWRSPGRGSWFVQALCSILE 250
TrCASP7-P10 210 NDTMETDANPRHKIPVEADFLFAYSTVPGYYSWRNPGRGSWFVQALCNVLS 261
HsCASP7-P10 251 EHGKDLEIMQILTRVNDRVARHFESQSDDPHFHEKKQIPCVVSMLTKELYF 301
TrCASP7-P10 262 EFGKQLEIMQILTRVNYMVATSFESWSEDPRFSEKKQIPCVVSMLTKELYF 312
B
HsCASP7
kDa – WT 205TME Y211H S234N S247N&I248V E250S H252F D255Q D267Y&R268M R271T&H272S Q276W D278E H281R H283S
72 55 43 34 26
FL
HsGSDME
CT
C
TrCASP7
kDa – WT 213ΔTME H221Y N245S N258S&V259I S261E F263H Q266D Y278D&M279R T282R&S283H W287Q E298D R292H S294H
72 55 43 34 26
FL
HsGSDME
CT
D
HsCASP7
kDa – WT 205TME Y211H S234N S247N&I248V E250S H252F D255Q D267Y&R268M R271T&H272S Q276W D278E H281R H283S
55 34 26
FL
TrGSDME
NT
CT
E
TrCASP7
kDa – WT 213ΔTME H221Y N245S N258S&V259I S261E F263H Q266D Y278D&M279R T282R&S283H W287Q E298D R292H S294H
55 34 26
FL
TrGSDME
NT
CT
F
WT S234N
kDa – 0.25 0.5 1 2 4 0.25 0.5 1 2 4 U
72 55 43 34 26
FL
HsGSDME
CT
G
kDa – WT S234N S234N+S247N&I248V Q276W&D278E &H283S
72 55 43 34 26
FL
HsGSDME
CT
H
kDa – WT S234N S234N+S247N&I248V Q276W&D278E &H283S
55 43 34 26
FL
TrGSDME
NT
CT
I
TrCASP7 HsCASP7
kDa – 60 120 250 500 60 120 250 500 (ng)
55 43 34
FL
HsGSDME
NT
55
CASP7
43
Actin
J
TrCASP7 HsCASP7
kDa – 60 120 250 500 60 120 250 500 (ng)
55 43 34
FL
TrGSDME
NT
55
CASP7
43
Actin
K
kDa – TrCASP7 TrCASP7-N245S HsCASP7 HsCASP7-S234N
55 43 34
FL
HsGSDME
NT
55
CASP7
43
Actin
L
kDa – TrCASP7 TrCASP7-N245S HsCASP7 HsCASP7-S234N
55 43 34
FL
TrGSDME
NT
55
CASP7
43
Actin
M
WT S234N
kDa – 60 120 250 500 60 120 250 500 (ng)
55 43 34
FL
HsGSDME
NT
55
CASP7
43
Actin

Figure 6

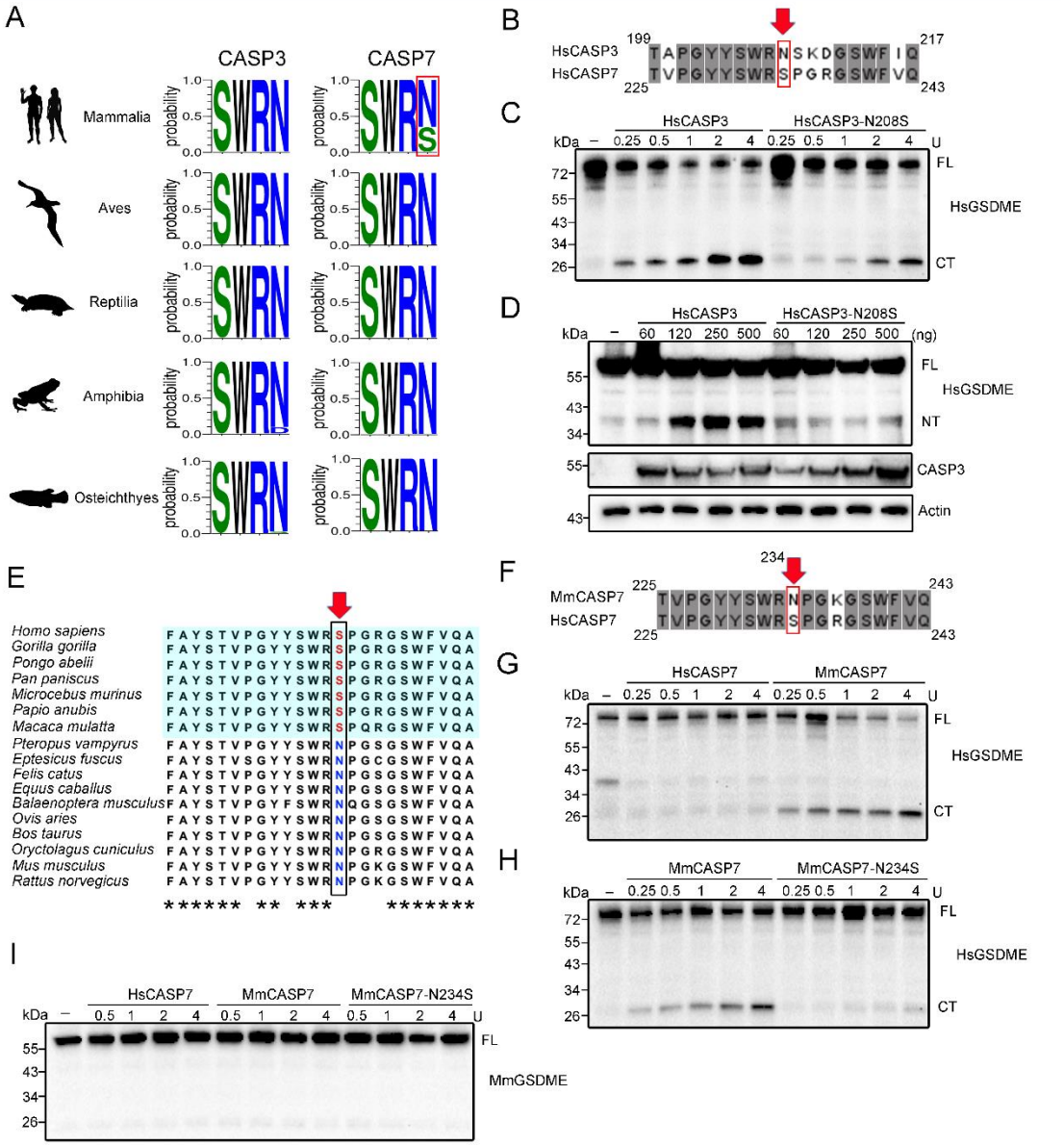
A
CASP3
CASP7
Mammalia
Aves
Reptilia
Amphibia
Osteichthyes
probability
B
HsCASP3
HsCASP7
C
HsCASP3
HsCASP3-N208S
HsGSDME
FL
CT
D
HsCASP3
HsCASP3-N208S
(ng)
HsGSDME
NT
CASP3
Actin
E
Homo sapiens
Gorilla gorilla
Pongo abelii
Pan paniscus
Microcebus murinus
Papio anubis
Macaca mulatta
Pteropus vampyrus
Eptesicus fuscus
Felis catus
Equus caballus
Balaenoptera musculus
Ovis aries
Bos taurus
Oryctolagus cuniculus
Mus musculus
Rattus norvegicus
F
MmCASP7
HsCASP7
G
HsCASP7
MmCASP7
HsGSDME
H
MmCASP7
MmCASP7-N234S
HsGSDME
I
HsCASP7
MmCASP7
MmCASP7-N234S
MmGSDME

Supplementary Materials

The file include:

Table S1. The credits for the pictures used in this study.

Table S2. Primers used in this study.

Fig. S1. Preparation of recombinant proteins.

Fig. S2. Conservation of S/N234 in mammalian CASP7.

Legends for S1 Movie.

Movie S1. TrGSDME-NT induces pyroptosis of HEK293T cells.

Table S1. The credits for the pictures used in this study.

Icons	Figure Origin
Monotremata	Becky-Barnes
Didelphimorphia	Daniel-Stadtmauer
Diprotodontia	Gavin-Prideaux
Afrosoricida	Mo-Hassan
Macroscelidea	uncredited
Pilosa	Xavier-A-Jenkins
Primates	T-Michael-Keesey
Rodentia	Jiro-Wada
Lagomorpha	Margot-Michaud
Eulipotyphla	Becky-Barnes
Perissodactyla	Mercedes-Yrayzoz-vectorized-by-T-Michael-Keesey
Artiodactyla	DFoidl-modified-by-T-Michael-Keesey
Carnivora	Chlo-Schmidt
Pholidota	Steven-Traver
Chiroptera	Margot-Michaud
Homo sapiens	NASA
Avian	Ferran Sayol
Reptilia	Gabriela Palomo-Munoz

Amphibia	Yusan Yang
Actinopterygii	Milton Tan

730 **Table S2. Primers used in this study.**

Primer	Sequence (5'-3')
Clone primers	
TrCASP3 forward	ATGTCGGCCAACGGACC
TrCASP3 reverse	GGAAAAATACATCTCTTTGGTCAGC
TrCASP7 forward	ATGCAGATGGCTGGAGAACC
TrCASP7 reverse	GTTAAAGTACAGTTCTTTTGTCAGCATCG
TrGSDME forward	ATGTTTTCCAAGGCCACGG
TrGSDME reverse	ATCGATAAAATCCGTTTCAGACTTTG
Recombiantion primers	
TrCASP3 forward	TAAGAAGGAGATATACATATGATGT CGGCCAACGGACC
TrCASP3 reverse	GTGGTGGTGGTGGTGCTCGAGGGA AAAATACATCTCTTTGGTCAGC
TrCASP7 forward	TAAGAAGGAGATATACATATGATGCA GATGGCTGGAGAACC
TrCASP7 reverse	GTGGTGGTGGTGGTGCTCGAGGTTAA AGTACAGTTCTTTTGTCAGCATCG
TrGSDME forward	TAAGAAGGAGATATACATATGATGTTT TCCAAGGCCACGG

TrGSDME reverse	GTGGTGGTGGTGGTGCTCGAGATCGA TAAAATCCGTTTCAGACTTTG
TrGSDME-D255R forward	TGGGAATCCCCGAGAGCGGTGGATGG TCGTTGTCT
TrGSDME-D255R reverse	AGACAACGACCATCCACCGCTCTCGG GGATTCCCA
TrGSDME-D258A forward	AGACAACGACCATCCACCGCTCTCGG GGATTCCCA
TrGSDME-D258A reverse	AACGACCATCCACCGCTCTCGGGGATT CCCA
HsNT-TrCT forward	TAAGAAGGAGATATACATATGATGTT TGCCAAAGCAACCAGG
HsNT-TrCT reverse	GTGGTGGTGGTGGTGCTCGAGATCG ATAAAATCCGTTTCAGACTTTG
TrNT-HsCT forward	TAAGAAGGAGATATACATATGATGTT TTCCAAGGCCACGG
TrNT-HsCT reverse	GTGGTGGTGGTGGTGCTCGAGTGAA TGTTCTCTGCCTAAAGC
Hsp20-Trp10 forward	TAAGAAGGAGATATACATATGATGG CAGATGATCAGGGCTG

Hsp20-Trp10 reverse	GTGGTGGTGGTGGTGCTCGAGGTTA AAGTACAGTTCTTTTGTCAGCATC
Trp20-Hsp10 forward	TAAGAAGGAGATATACATATGATGG CTGGAGAACCCACTGAG
Trp20-Hsp10 reverse	GTGGTGGTGGTGGTGCTCGAGTTGA CTGAAGTAGAGTTCCTTGGTGA
MmGSDME-N234S forward	GTTATTACTCATGGAGGAGCCCAGG GAAAG
MmGSDME-N234S reverse	CTTTCCCTGGGCTCCTCCATGAGTA ATAAC
HsGSDME-Δ261-266 forward	CCAGGATGGACATCCATTTGCGGAG CTGC
HsGSDME-Δ261-266 reverse	CAAATGGATGTCCATCCTGGGAAGAT ATCCCAT
HsGSDME-Δ281-296 forward	CCTGGTCTTT GACATGCCAGATGCTG CGCA
HsGSDME-Δ281-296 reverse	CTGGCATGTCAAAGACCAGGGGGTCC AGGTAGA
Overexpression preimers	
TrGSDME-FL forward	TCAGATCTCGAGCTCAAGCTTATGTTT

TrGSDME-FL reverse	TCCAAGGCCACGG
	CATGGTGGCGACCGGTGGATCATCGA
TrGSDME-NT forward	TAAAATCCGTTTCAGACTTTG
	TCAGATCTCGAGCTCAAGCTTATGTTT
TrGSDME-NT reverse	TCCAAGGCCACGG
	CATGGTGGCGACCGGTGGATCGTCTAC
TrGSDME-CT forward	AGCATCAGGAGACTCC
	TCAGATCTCGAGCTCAAGCTTATGGGCC
TrGSDME-CT reverse	GGTGCCTGGA
	CATGGTGGCGACCGGTGGATCATCGA
TrCASP7 forward	TAAAATCCGTTTCAGACTTTG
	TTCTGAAGAGGACTTGAATTCAATGG
TrCASP7 reverse	CTGGAGAACCCACTGAG
	ACGACTCACTATAGTTCTAGATCAGT
TrCASP3 forward	TAAAGTACAGTTCTTTTGTCAGC
	TTCTGAAGAGGACTTGAATTCAAATG
TrCASP3 reverse	TCGGCCAACGGACC
	ACGACTCACTATAGTTCTAGAGGAA
HsGSDME forward	AAATACATCTCTTTGGTCAGC
	CAAGCTTGCGGCCGCGAATTCAATGT

HsGSDME reverse	TTGCCAAAGCAACCAGG
	ACGACTCACTATAGTTCTAGATCATG
HsCASP7 forward	AATGTTCTCTGCCTAAAGC
	TTCTGAAGAGGACTTGAATTCAATGG
HsCASP7 reverse	CAGATGATCAGGGCTG
	ACGACTCACTATAGTTCTAGACTATTG
HsCASP3 forward	ACTGAAGTAGAGTTCCTTGGTG
	TTCTGAAGAGGACTTGAATTCAATGG
HsCASP3 reverse	AGAACACTGAAAACTCAGTGG
	ACGACTCACTATAGTTCTAGATTAGTG
MmCASP7 forward	ATAAAAATAGAGTTCTTTTGTGAGC
	TTCTGAAGAGGACTTGAATTCAATGA
MmCASP7 reverse	CCGATGATCAGGACTGTGC
	ACGACTCACTATAGTTCTAGATCAAC
	GGCTGAAGTACAGCTCTTTGG

Fig. S1. Preparation of recombinant proteins. (**A**) SDS-PAGE analysis of purified Hsp20-Trp10 and Trp20-Hsp10. (**B, C**) Recombinant mutants of TrCASP7 (B) and HsCASP7 (C) were purified and subjected to SDS-PAGE. (**D**) HsCASP3 and its mutant (N208S) were analyzed by SDS-PAGE. (**E**) SDS-PAGE analysis of purified MmCASP7 and its mutant (N234S). In all panels, the p10 and p20 subunits are indicated.

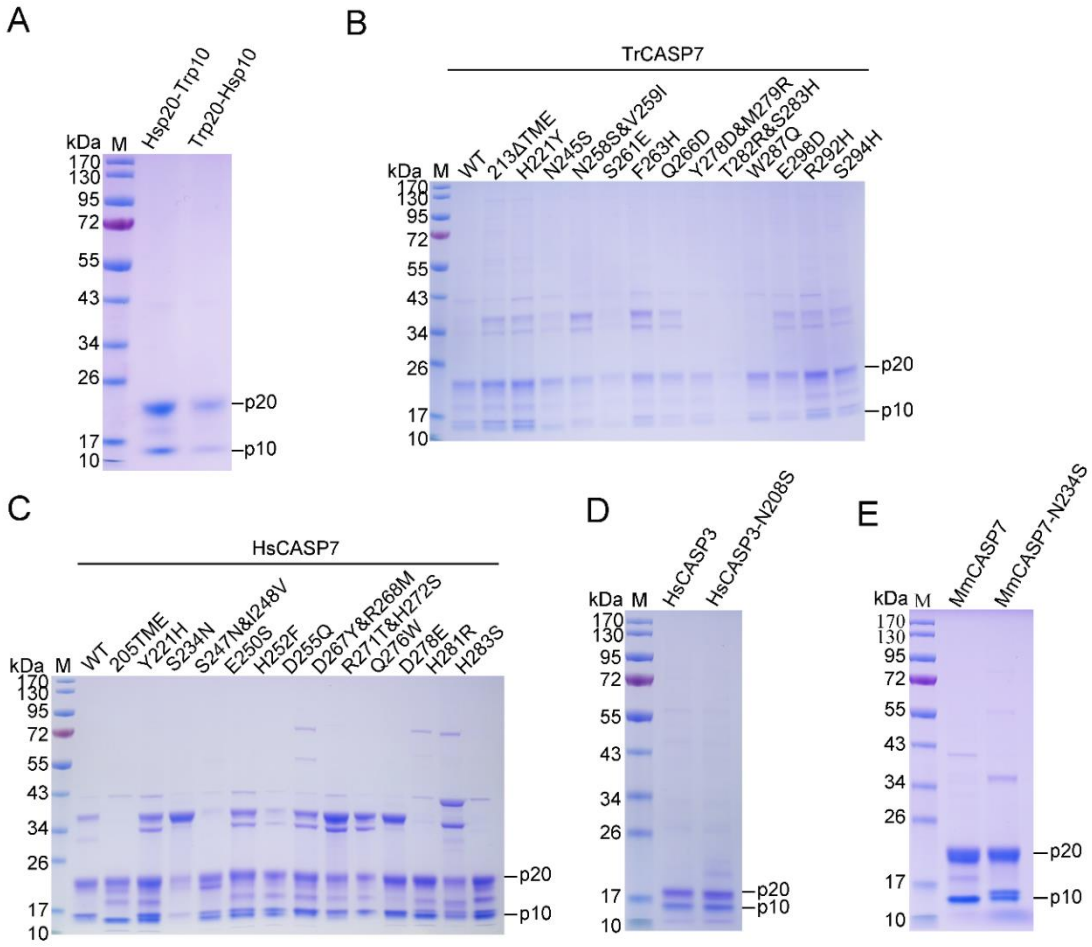

Fig. S2. Conservation of S/N234 in mammalian CASP7. The four conserved amino acids are shown in LOGOs, with height representing the relative proportion of the corresponding amino acid at that position. The S/N234 is presented as the fourth LOGO and indicated with a red star.

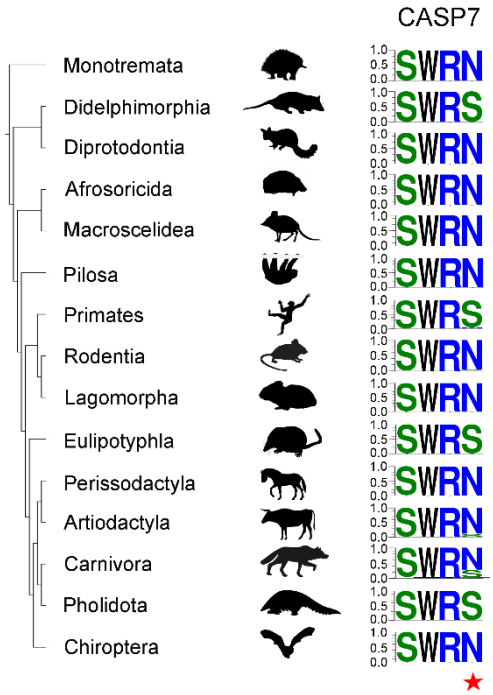

Movie S1 (separate file). TrGSDME-NT induces pyroptosis of HEK293T cells. HEK293T cells were transfected with the vector expressing mCherry-tagged TrGSDME-NT, and time-lapse images of the cells were recorded with a Carl Zeiss LSM 710 confocal microscope.